Direct observation of the particle-phase bicyclic products from OH-initiated oxidation of 1,3,5-trimethylbenzene under NOx-free conditions

Xiaoxiao Lin, Xiaofeng Tang, Zuoying Wen, Bo Long, Christa Fittschen, Xuejun Gu, Yanbo Gai, Weijun Zhang

Atmospheric Environment xxx (xxxx) 118914

Contents lists available at ScienceDirect

Atmospheric Environment

journal homepage: www.elsevier.com/locate/atmosenv

Direct observation of the particle-phase bicyclic products from OH-initiated oxidation of 1,3,5-trimethylbenzene under NOx-free conditions

Xiaoxiao Lin [a], Xiaofeng Tang [a, *], Zuoying Wen [a], Bo Long [b, **], Christa Fittschen [c], Xuejun Gu [a], Yanbo Gai [a], Weijun Zhang [a, ***]

[a] Laboratory of Atmospheric Physico-Chemistry, Anhui Institute of Optics and Fine Mechanics, HFIPS, Chinese Academy of Sciences, Hefei, 230031, Anhui, China
[b] School of Materials Science and Engineering, Guizhou Minzu University, Guiyang, 550025, Guizhou, China
[c] University Lille, CNRS, UMR 8522, PC2A – Physicochimie des Processus de Combustion et de l'Atmosphère, F-59000, Lille, France

ARTICLE INFO

Keywords:
1,3,5-Trimethylbenzene
The bicyclic peroxy radical
Secondary organic aerosol
Vacuum ultraviolet photoionization
Aerosol mass spectrometry

ABSTRACT

The OH initiated oxidation of 1,3,5-trimethylbenzene (1,3,5-TMB) under NOx-free conditions has been investigated by using a home-made vacuum ultraviolet (VUV) photoionization aerosol mass spectrometer complemented by high-level theoretical computations. The chemical composition of the nascent particles from the oxidation reaction is measured on-line and the high mass O_2-bridged bicyclic compounds in the particle phase are directly observed and determined, with the aid of the deuterated 1,3,5-TMB experiments to confirm the species' assignment. To illuminate the formation of the O_2-bridged bicyclic compounds, the potential energy surfaces of the reaction of the bicyclic peroxy radical (BPR) with the hydroperoxy radical (HO_2), and of the self-reaction of the BPR radical, have been theoretically calculated and then their reaction mechanisms are discussed in detail. This study provides direct evidence to support the essential role of the O_2-bridged bicyclic compounds in the particle formation from the OH initiated oxidation of 1,3,5-TMB.

1. Introduction

Volatile organic compounds (VOCs) emitted into the atmosphere from a variety of biogenic and anthropogenic sources are the major precursors of secondary organic aerosols (SOA), which is known to affect visibility, climate and human health (Hallquist et al., 2009; Kroll and Seinfeld, 2008). In particular, aromatic VOCs such as benzene, toluene and xylene can make up 13–44% of the total hydrocarbons in the urban atmosphere and play an essential role in the formation of SOA (Dommen et al., 2003; Molina et al., 2007; Vega et al., 2011). Concretely, the atmospheric oxidation of these aromatic VOCs can yield a multitude of oxygenated products with a high mass and a low volatility, and then contribute to the SOA formation and growth.

1,3,5-trimethylbenzene (1,3,5-TMB, C_9H_{12}) is a significant aromatic compound and mostly emitted from automobile exhaust, solvent use and industry (Velasco et al., 2007). In the atmosphere, the oxidation of 1,3,5-TMB is mainly initiated by the hydroxyl radical (OH) with a reaction rate constant of $k_{298K} = (5.67 \pm 1.14) \times 10^{-11}$ cm^3 molecule^{-1} s^{-1} (Aschmann et al., 2006), and has attracted attention in the past decades. With the constant development of various analytical techniques, the major gas-phase products of the oxidation of 1,3,5-TMB and the most composition of its SOA have been identified and characterized in experiments. The embedded complex oxidation mechanism of 1,3,5-TMB has been unraveled and added in chemical models like the Master Chemical Mechanism (MCM), (Bloss et al., 2005; Jenkin et al., 2003).

The reaction of 1,3,5-TMB with OH can occur via two routes, the hydrogen abstraction and the OH addition routes. Presently it is believed that the OH addition to the aromatic ring of 1,3,5-TMB is the major reaction route with a branching ratio of 97%, based on the mechanisms of the MCM 3.3.1 (Jenkin et al., 2003; Ponnusamy et al., 2017), and the hydrogen abstraction is the minor route with a ratio of 3%. In the presence of oxygen, the nascent OH-1,3,5-TMB adduct (B) will react with oxygen to generate the OH-1,3,5-TMB-O_2 peroxy radical (C), as shown in Fig. 1. Then the OH-1,3,5-TMB-O_2 peroxy radical (C) can perform isomerization, react with oxygen again and cyclize to produce the bicyclic peroxy radical (BPR, D).

In the atmosphere, peroxy radicals can react with various species such as NOx (NO and NO_2), HOx (OH and HO_2) and other peroxy radi-

* Corresponding author.
** Corresponding author.
*** Corresponding author.
E-mail addresses: tangxf@aiofm.ac.cn (X. Tang), longbo@gzmu.edu.cn (B. Long), wjzhang@aiofm.ac.cn (W. Zhang).

https://doi.org/10.1016/j.atmosenv.2021.118914
Received 2 September 2021; Received in revised form 26 November 2021; Accepted 16 December 2021
1352-2310/

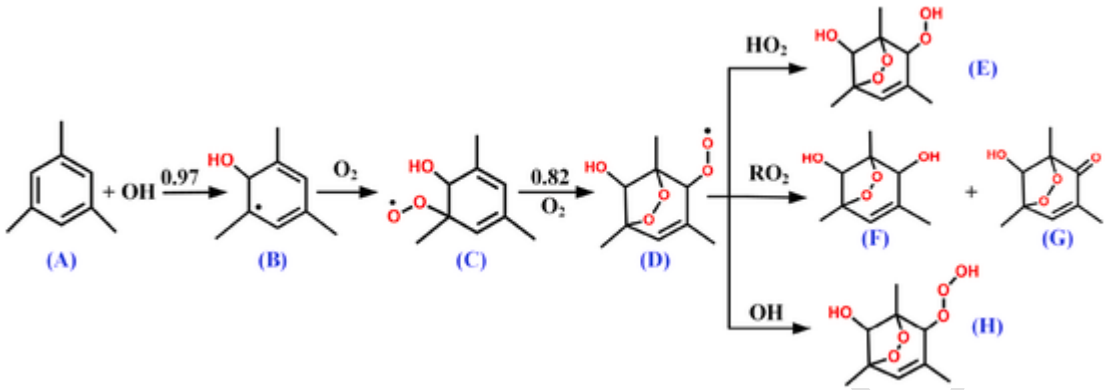

Fig. 1. The major reaction routes of the OH initiated photo-oxidation of 1,3,5-TMB under NOx free conditions. The reaction intermediates and products, together with the branching ratios, are taken from MCM 3.3.1 (http://mcm.leeds.ac.uk/MCM). The reaction pathway between the bicyclic peroxy radical (D) and the OH radical has also been added.

cals (RO_2) dependent on the sites and real conditions (Orlando and Tyndall, 2012). For example, under low NOx condition, peroxy radicals will mainly react with the HO_2 radical and other peroxy radicals, as well as performing their self-reaction, while at high-NOx condition the RO_2 + NOx reaction is the predominant. The gas-phase bicyclic products from the reactions of the BPR radical were observed by Wyche et al. using chemical ionization mass spectrometry (CIMS) and in their experiments low NOx conditions can favor more rapid aerosol formation with a high yield (Wyche et al., 2009). Presently, under low NOx conditions, it is believed that the BPR radical will react with HO_2 to form the O_2-bridged bicyclic peroxide (E), and the BPR radical can also perform self-reaction to form the products of the bicyclic alcohol (F) and the bicyclic carbonyl (G), as shown in Fig. 1. These bicyclic products have a high mass with a low volatility, and thus should play an essential role in the formation of SOA. Moreover, these bicyclic products can undergo further oxidation in the atmosphere to form highly oxygenated organic molecules (HOMs), which have been identified recently with CIMS too (Mehra et al., 2020; Wang et al., 2020).

Fittschen et al. studied the reactions of alkyl peroxy radicals with OH and found the RO_2+OH reaction has a large rate constant ($\sim 10^{-10}$ cm^3 $molecule^{-1}$ s^{-1}), which should be considered as an important reaction under low NOx conditions (Assaf et al., 2016; Faragó et al., 2015; Yan et al., 2016). The reaction of RO_2 with OH can produce the trioxide adduct (ROOOH) and its branching ratio increases with the size of RO_2 and even can approach unity for larger RO_2 (Assaf et al., 2018). Recently, the authors of this manuscript performed theoretical calculations on the reaction of the BRP radical with OH, and found the reaction rate constant is large too, at 1.88×10^{-11} cm^3 $molecule^{-1}$ s^{-1} at 298 K. In addition, the trioxide adduct (H) was predicted to be the major product of the reaction (Lin et al., 2019). These results indicate that the reaction of the BPR radical with OH could also take some role in the oxidation of 1,3,5-TMB under NOx-free conditions.

In this work, the OH-initiated oxidation of 1,3,5-TMB under NOx-free conditions has been investigated in an atmospheric simulation chamber coupled to a detection using a vacuum ultraviolet (VUV) photoionization aerosol mass spectrometer. Experiments were complemented by high-level theoretical computations. The chemical composition of the nascent particles in the oxidation reactions was measured on-line and the above mentioned O_2-bridged bicyclic products with a high mass and a low volatility were detected in the particle phase, which directly demonstrates that they took part into the formation of particles. In addition, to confirm the products and to reveal the reaction mechanisms in detail, the oxidation experiments were also performed with deuterated 1,3,5-TMB (1,3,5-TMB-d_{12}, C_9D_{12}) samples. Theoretical computations confirmed the reaction pathways. This work will provide a detailed insight into the reaction mechanisms of the BPR radical contributing to the SOA formation during the OH-initiated oxidation of 1,3,5-TMB.

2. Methods

2.1. Experimental setup

The experimental setup mainly consists of three parts—an atmospheric simulation chamber, a commercial scanning mobility particle sizer (SMPS, TSI 3963, USA) and a home-made VUV photoionization aerosol mass spectrometer—and its schematic diagram is displayed in Fig. 2. The configuration of the setup has been described in detail in our recent publication (Wen et al., 2020a) and only a brief description is presented here.

The simulation chamber is made of a 0.15 m^3 Teflon bag surrounded by six UV lamps (Philips TUV G13, 36 W) emitting photons with wavelengths at around 254 nm and employed as a chemical reactor to simulate the atmospheric reactions (Gai et al., 2015). 1,3,5-TMB (98%, Alfa Aesar) or 1,3,5-TMB-d_{12} (98 atom% D, Sigma Aldrich) was delivered into the Teflon bag via a heated injector port and zero air from a pure air generator (AADCO 737-series) was added into as bath gas. H_2O_2 (35%, Acros Organics) was injected into the Teflon bag as the precursor to produce the OH radical via the UV photolysis and then to

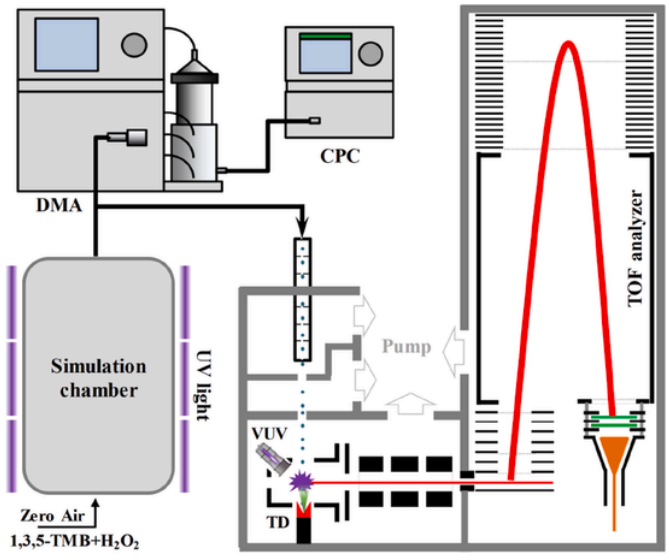

Fig. 2. Schematic diagram of the setup, mainly consisting of an atmospheric simulation chamber, a scanning mobility particle sizer (SMPS), and a vacuum ultraviolet (VUV) photoionization aerosol mass spectrometer.

initiate the reactions. The initial concentrations of 1,3,5-TMB and 1,3,5-TMB-d_{12} inside the Teflon bag are estimated at 800 ppb, and the experiments are performed at room temperature (~298 K). The commercial SMPS, consisting of a differential mobility analyzer (DMA, TSI 3081) and a condensation particle counter (CPC, TSI 3776), is used to measure the size distribution of the nascent particles inside the Teflon bag.

The VUV photoionization aerosol mass spectrometer is adopted to measure the chemical composition of the particles on-line and is mainly composed of four vacuum chambers: a source chamber, a differential chamber, a photoionization chamber and a time-of-flight (TOF) chamber, as shown in Fig. 2. An aerodynamic lens (ADL) installed in the source chamber is used to sample and focus particles into the vacuum chambers of the mass spectrometer. The ADL consists of several thin plates and spacers, and the diameter of its entrance orifice is 100 μm, with a flow rate of 100 cm^3 min^{-1} into the mass spectrometer. After passing through two skimmers (1 mm diameter, Beam Dynamics, Inc.), the focused particles arrive on the hot surface of a thermal desorption (TD) module, and then are flash-vaporized into gas-phase molecules after absorbing the heat. The TD module is made of porous tungsten and its temperature was set at 250 °C, which is high enough to vaporize most organic compounds.

A krypton discharge lamp (PKS106, Heraeus, Germany) with photon energies at $h\nu$ = 10.0 and 10.6 eV is employed as the VUV photoionization light source. As shown in Fig. 2, the flash-vaporized molecules cross the VUV light in the photoionization chamber at a right angle and gas-phase molecules having an ionization energy of less than 10.6 eV can be ionized. A compact orthogonal acceleration reflectron TOF mass analyzer is employed to analyze the mass of ions. In addition, a cage-shaped photoionization source has been developed to enhance the detection sensitivity and an Einzel lens with three cylindrical tubes is installed to focus and transmit ions (Wen et al., 2020b). Then, after passing through a 2 × 6 mm^2 slit connecting the photoionization chamber and the TOF chamber, the ions are orthogonally accelerated by a dual-pulse voltage into a field-free region and then reflected by a two stages reflector. Finally, ions are detected by a pair of microchannel plates (MCPs; 50 mm diameter) in a chevron configuration. The total flying length of ions in the photoionization mass spectrometer is about 1 m and its mass resolution (M/△M) is ~2100 (FWHM, full width at half magnitude).

2.2. Theoretical computations

Potential energy surfaces are calculated for the bimolecular reactions of the BPR radical to examine the formation pathways leading to the observed bicyclic products. Concretely, the potential energy surfaces of the reaction of the BPR radical with HO_2 are computed at the CCSD(T)-F12a/cc-pVDZ-F12//M062X/MG3S level of theory. For the self-reaction of the BPR radical, the DFT M06–2X method with the 6–31g(d,p) basis set is employed for the calculation of this large reaction system. For the reaction of the BPR radical with HO_2, the structural optimizations and the vibrational frequency analyses are conducted by using the Gaussian 16 program package (Frisch et al., 2016), and the energies of the reactants, the transition states and the products are calculated by using the Molpro 2012.1 package (Werner and Knowles, 2012).

The reaction rate constants are evaluated by the conventional transition-state theory (CTST) (Fernández-Ramos et al., 2006; Steinfeld et al., 1999), which is performed with the TheRate program (Duncan et al., 1998; Zhang and Truong, 2001). For the self-reaction of the BPR radical, the calculations of molecular parameters are performed by using the Gaussian 16 package too. The intrinsic reaction coordinate (IRC) calculations are also carried out to confirm the transition states connecting the reactants and products (Gonzalez and Schlegel, 1989, 1990). The adiabatic ionization energy (AIE) of the 1,3,5-TMB trioxide species is calculated at the CCSD(T)-F12a/cc-pVDZ-F12//M06–2X/MG3S level of theory with the Gaussian 16 and the Molpro packages.

3. Results and discussion

3.1. Particle size distributions

In the OH-initiated oxidation reaction of 1,3,5-TMB, many products have been formed and observed, and gas-phase products with a low volatility can take part into the nucleation process to produce new particles and SOA. Fig. 3(a) shows the particle size distribution inside the Teflon bag. We can see that at the beginning without turning on the UV lamps (time <12 min) only background signals can be observed. After turning on the UV lamps, the oxidation reaction of 1,3,5-TMB was initiated with the OH radical produced via the UV photolysis of H_2O_2. Almost at the same time new particles were formed and its diameter and concentration increased with reaction time. The deuterated 1,3,5-TMB-d_{12} experiment has also been performed under the same conditions and its particle size distribution is presented in Fig. 3(b), whose shape is very similar to that of the 1,3,5-TMB experiment. We can see that, for the both experiments, the particle diameter increased quickly with time at the beginning and then approached a steady state at ~20 min, with its mean diameter at ~180 nm.

3.2. Chemical composition of particles

Photoionization mass spectra of the particles formed in the OH-initiated oxidation reactions of 1,3,5-TMB are measured with the VUV photoionization aerosol mass spectrometer and a representative of them with its high mass part has been chosen and displayed in Fig. 4(a). A large number of peaks can be observed in the mass spectrum and its

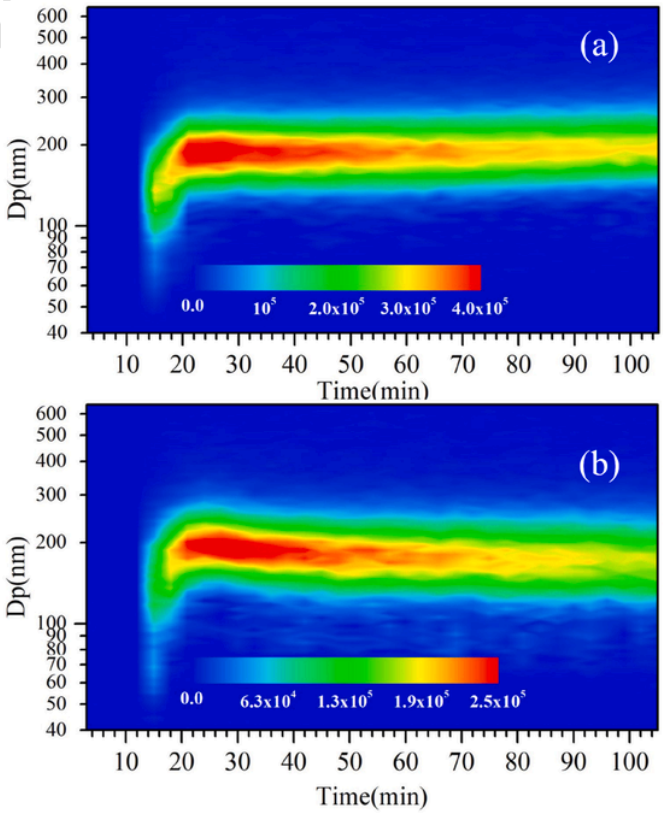

Fig. 3. The particle size distribution in the OH-initiated oxidation experiments of (a) 1,3,5-TMB (C_9H_{12}) and (b) the deuterated 1,3,5-TMB (C_9D_{12}). The UV lamps were turned on at ~12 min to start the reactions.

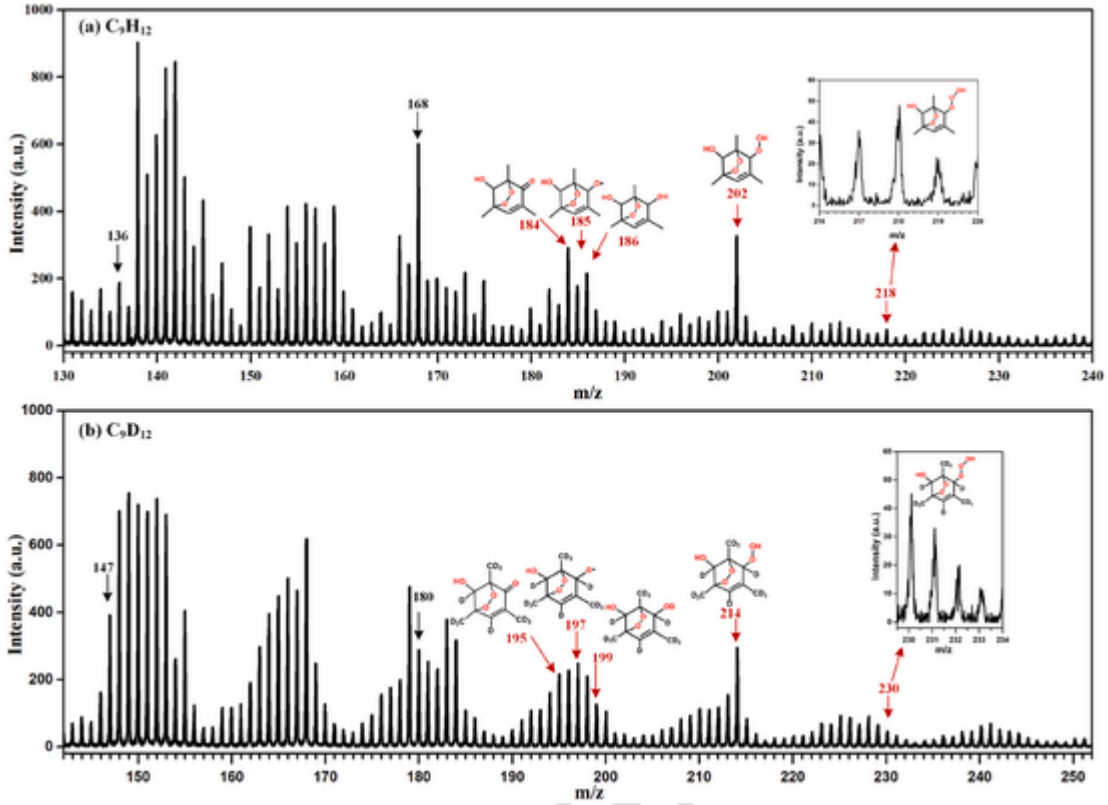

Fig. 4. VUV photoionization mass spectra of particles from the OH-initiated oxidation of (a) 1,3,5-TMB and (b) the deuterated 1,3,5-TMB (C_9D_{12}) under NOx-free conditions.

overall shape agrees with previous results (Ma et al., 2018). With the help of literature data of Ma et al., the mass peaks of Fig. 4(a) can be assigned and their major assignments have been listed in Table 1 of Lin et al. (2021). Presently, due to the high mass resolution of the setup, some delicate information can be unraveled in particular for the high mass species.

Table 1
Molecular structures of the O_2-bridged bicyclic products from oxidation of 1,3,5-TMB and deuterated 1,3,5-TMB-d_{12}.

Bicyclic product			Deuterated Bicyclic Products		
Name	m/z	Structure	Name	m/z	Structure
1,3,5-trimethyl-6,7-dioxa-bicyclo[3.2.1] oct-3-ene-2,8-diol	186	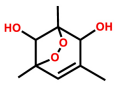	1,3,5-trimethyl-6,7-dioxa- bicyclo [3.2.1] oct-3-ene-2,d8-diol-d_{13}	199	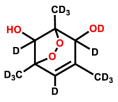
8-hydroxy-1,3,5-trimethyl-6,7-dioxa-bicyclo [3.2.1] oct-3-en-2-hydroperoxide	202	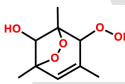	8-hydroxy-1,3, 5-trimethyl-6, 7-dioxa-bicyclo [3.2.1] oct-3-en-2-hydroperoxide-d_{12}	214	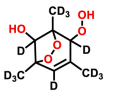
8-hydroxy-1,3,5-trimethyl-6,7-dioxa-bicyclo [3.2.1] oct-3-en-2-one	184	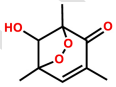	8-hydroxy-1,3, 5-trimethyl-6, 7-dioxa-bicyclo [3.2.1] oct-3-en-2-one-d_{11}	195	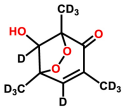
8-hydroxy-1,3,5-trimethyl-6,7-dioxa-bicyclo [3.2.1]oct -3-en-2-trioxide	218	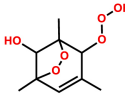	8-hydroxy-1,3, 5-trimethyl-6, 7-dioxa-bicyclo [3.2.1]oct -3-en-2-trioxide-d_{12}	230	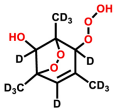

Under NOx-free conditions, the BPR radical (D) will perform self-reaction or bimolecular reaction with HO_2 or with other peroxy radicals, and then the O_2-bridged bicyclic oxygenated compounds can be formed, as shown in Fig. 1. For example, the self-reaction of the BPR radical can generate the products of the O_2-bridged bicyclic alcohol (F, m/z = 186) and the O_2-bridged bicyclic carbonyl (G, m/z = 184), and the bimolecular reaction of the BPR radial with HO_2 can produce the O_2-bridged bicyclic peroxide (E, m/z = 202). These O_2-bridged bicyclic oxygenated compounds have already been observed in the gas-phase in previous CIMS experiments (Wyche et al., 2009). Due to their high masses and low volatilities, these O_2-bridged bicyclic oxygenated compounds should get into the particle phase and play an essential role in the particle formation.

Based on the above discussion, the peaks at m/z = 184, 186 and 202 in the mass spectrum of Fig. 4(a) should be assigned as the O_2-bridged bicyclic carbonyl (G), alcohol (F) and peroxide (E), respectively, also as shown in Table 1. To confirm these assignments, a photoionization mass spectrum of the particles from the OH-initiated oxidation of deuterated 1,3,5-TMB-d_{12} (C_9D_{12}) has also been measured and is presented in Fig. 4(b). The overall shape of the mass spectrum is similar to that of Fig. 4(a), with a mass shift of 12 amu, in accordance with the isotopic effect. Concretely, now the mass peak at m/z = 214 in Fig. 4(b) can be assigned as the deuterated O_2-bridged peroxide, in accordance with the O_2-bridged peroxide at m/z = 202 in Fig. 4(a). The deuterated O_2-bridged ketone locates at m/z = 195, and the deuterated O_2-bridged diol is at m/z = 199. The chemical compositions of particles observed in the photoionization mass spectra clearly demonstrate that the nascent O_2-bridged bicyclic oxygenated compounds from the BPR radical reactions have entered into the particle phase.

In addition, a great deal of other peaks, besides the above bicyclic products, can be observed and assigned in the mass spectra of Fig. 4.

For example, the ring retaining products of 3,5-dimethylbenzaldehyde (m/z = 134) and 2,4,6-trimethylphenol (m/z = 136) are identified, and the epoxy-oxy compound (m/z = 168) formed from the isomerization and decomposition reactions of the OH-aromatic-O_2 adduct radical (C) can be clearly observed in the particle phase. Further decomposition of the epoxy-oxy compound can yield a variety of lower mass oxygenates too. Moreover, the ring cleavage of the O_2-bridged bicyclic ketone (m/z = 184) and the alkoxy radical will also yield an array of low mass oxygenated compounds, some of which have been listed in Table 1 of Lin et al. (2021).

3.3. Reaction mechanisms of the BPR radical

To illuminate the detailed mechanisms for the formation of the above O_2-bridged bicyclic oxygenated compounds, the reaction pathways of the BPR radical with HO_2 and its self-reaction have been theoretically studied. For the bimolecular reaction of the BPR radical with HO_2, the potential energy surfaces are calculated at the CCSD(T)-F12a/cc-pVDZ-F12//M06–2X/MG3S level of theory with the Gaussian 16 and Molpro 2012.1 packages, and presented in Fig. 5. The theoretical calculations show that the reaction is occurred along a triplet potential energy surface via the hydrogen abstraction of the HO_2 radical to form the O_2-bridged bicyclic hydroperoxide (E, $C_9H_{14}O_5$) and $^3O_2$ products, whereas the reaction routes along the singlet potential energy surfaces are accompanied with high barriers, which are too high to be overcome at room temperature. The optimized structures of the reaction intermediates and the transition states are shown in Fig. 2 of Lin et al. (2021). The reaction rate constant of the BPR radical with HO_2 is calculated at 5.72 × 10^{-14} cm^3 $molecule^{-1}$ s^{-1} by using the transition state theory (Eyring, 1935; Truhlar et al., 1996). The theoretical calculations demonstrate that the formation of the O_2-bridged bicyclic hydroperoxide (E) and $^3O_2$ products is the most feasible route in the reaction of the BPR radical with HO_2.

To explain the formation of the O_2-bridged bicyclic alcohol (F) and ketone (G) products, theoretical calculations are also conducted on the self-reaction of the BPR radical. Previous results (Hasan et al., 2020) show that the self-reaction of peroxy radicals is proceeded with an intermediate complex ^{1}(RO … $^3O_2$ … OR) and this weakly bound complex can easily evaporate its center component $^3O_2$ to produce a triplet-state dimer of alkoxy radicals ^{3}(RO … OR). Based on the results, the structure of the dimer ^{3}(TMB-RO … OR-TMB) of the BPR radical has been optimized at the M06–2x/6-31g(d,p) level of theory. The energetic parameters including the reaction energy and the barrier height are also calculated for the hydrogen-shift reaction of the dimer ^{3}(TMB-RO … OR-TMB), leading to the formation of the O_2-bridged bicyclic alcohol (F) and ketone (G), as shown in Fig. 6.

The dimer ^{3}(TMB-RO … OR-TMB) is a H-bonded complex with the bond distance of its two monomers at 2.437 Å (Å), which favors the unimolecular H-shift. The reaction barrier is calculated to be at −0.93 kcal mol^{-1} via an H-shift transition state (^{3}TS). The C–H and O–H bond lengths of the ^{3}TS transition state are calculated at 1.186 and 1.429 Å, respectively. The structures of the O_2-bridged bicyclic alcohol (F, ROH) and ketone (G, $^3R_{-H}$═O) are also optimized and presented in Fig. 6, with the reaction energies calculated at −19.19 kcal mol^{-1}, also indicating the reaction is energetically favorable. For the deuterated ^{3}(TMB-RO … OR-TMB), the deuterium-shift reaction leads to the formation of the deuterated O_2-bridged ketone (m/z = 195) and the deuterated O_2-bridged diol (m/z = 199), as shown in Fig. 3 of Lin et al. (2021). Thus, the bicyclic products from the self-reaction of the deuterated BPR radical are observed with an odd mass number in the mass spectrum of Fig. 4(b).

In addition to the above mentioned reaction of the BPR radical with HO_2 and its self-reaction, the BPR radical might also perform bimolecular reaction with the OH radical under the NOx-free conditions (Fittschen et al., 2014). Recently, the authors of this work also carried out theoretical computations on the reaction of the BPR radical with OH, and the rate constant was calculated to be 1.88 × 10^{-11} cm^3 $molecule^{-1}$ s^{-1} at 298 K, larger than that of the BPR radical with HO_2 (6.88 × 10^{-13} cm^3 $molecule^{-1}$ s^{-1}) (Lin et al., 2019). So the reaction of the BPR radical with OH could be important too in the oxidation of 1,3,5-TMB. The theoretical calculations also show that the major product of the BPR radical reaction with OH is the 1,3,5-TMB trioxide (H, ROOOH).

The products of the 1,3,5-TMB trioxide and the deuterated 1,3,5-TMB trioxide are expected to locate at m/z = 218 and 230 in the mass spectra of Fig. 4(a) and (b). The lack of the intense signal of the 1,3,5-TMB trioxide product in the mass spectra can be partially explained by its photoionization characters. The adiabatic ionization energies (AIEs)

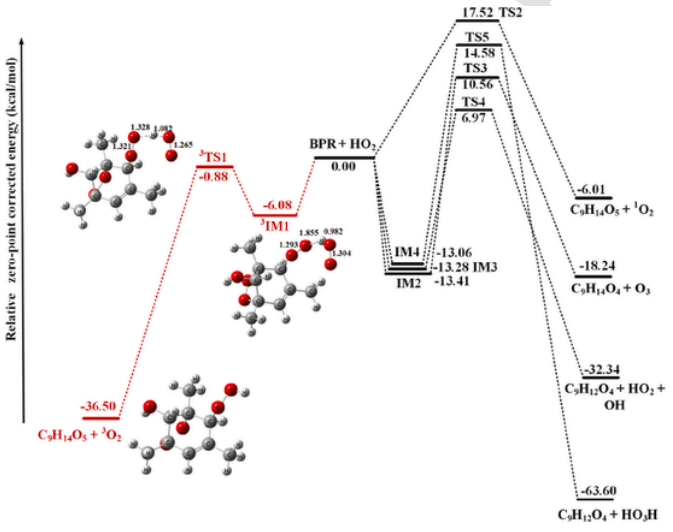

Fig. 5. Potential energy surfaces of the reaction of the O_2-bridged bicyclic peroxy radical (BPR) with HO_2 calculated at the CCSD(T)-F12a/cc-pVDZ-F12//M062X/MG3S level of theory. The singlet reaction pathways are depicted in black, and the triplet one in red. (For interpretation of the references to colour in this figure legend, the reader is referred to the Web version of this article.)

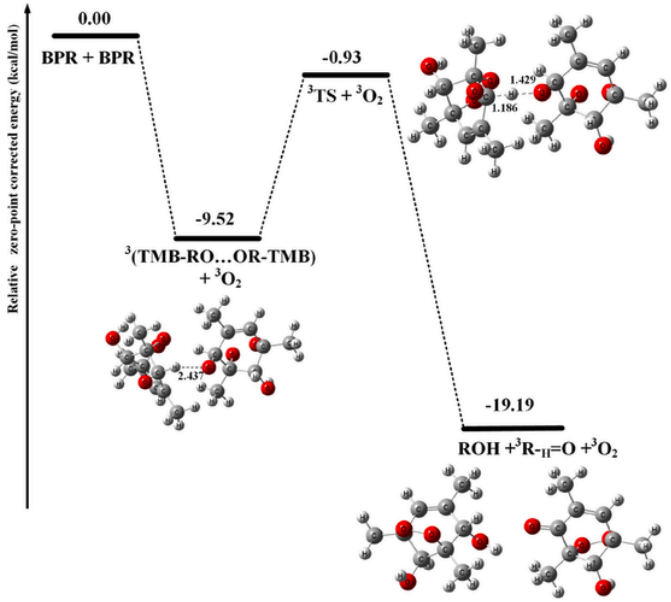

Fig. 6. Potential energy surface of the ^{3}(TMB-RO···OR-TMB) → ROH + R_{-H}═O reaction and the optimized structures at the M06–2X/6-31g (d,p) level. Color coding: gray, C; white, H; red, O. (For interpretation of the references to colour in this figure legend, the reader is referred to the Web version of this article.)

of the 1,3,5-TMB trioxide and the deuterated 1,3,5-TMB trioxide products are calculated at 8.68 eV at the CCSD(T)-F12a/cc-pVDZ-F12//M06–2X/MG3S level of theory, far below the VUV photon energy of 10.6 eV. So, in the photoionization, the nascent trioxide cation is produced with a high internal energy and will dissociate into the RO^+ and HO_2 fragments. The m/z = 185 peak in the mass spectrum of Fig. 4 (a) and the m/z = 197 peak in Fig. 4(b) should have contributions of the trioxide and the deuterated trioxide cations. Another possible explanation is that the trioxide does not survive and decomposes to the ROH (m/z = 186) and O_2 fragments either on the chamber walls or on the sampling tube (Caravan et al., 2018), which are deserved to be studied in detail in the future.

4. Conclusions

In this work, we present a combined experimental and theoretical study of the OH-initiated oxidation of 1,3,5-TMB under NOx-free conditions in an atmospheric simulation chamber. The chemical composition of the nascent particles is measured on-line by using a home-made VUV photoionization aerosol mass spectrometer. Many species, in particular the high-mass O_2-bridged bicyclic products, have been clearly observed in the particle phase and determined in the photoionization mass spectra, with the aid of the deuterated experiments to confirm the species' assignments. It is shown that the O_2-bridged bicyclic peroxy radical is the key intermediate in the oxidation of 1,3,5-TMB and can perform various reactions including its self-reaction, the bimolecular reaction with the HO_2 radical, and the reaction with the OH radical. Due to the high mass and low volatility, these reaction products can enter into the particle phase and become important components of the nascent particle. Moreover, the reaction pathways of the BPR radical have been theoretically calculated and their mechanisms are also discussed. The present results give direct evidences of the peroxy radical chemistry in the new particle formation and the SOA formation, in particular the reactions involving the multi-functional O_2-bridged oxidation products.

CRediT authorship contribution statement

Xiaoxiao Lin: Conceptualization, Methodology, Investigation, Writing – original draft. **Xiaofeng Tang:** Conceptualization, Methodology, Investigation, Funding acquisition, Project administration, Visualization, Writing – review & editing. **Zuoying Wen:** Investigation. **Bo Long:** Formal analysis, Investigation. **Christa Fittschen:** Writing – review & editing. **Xuejun Gu:** Investigation. **Yanbo Gai:** Investigation. **Weijun Zhang:** Resources, Supervision.

Declaration of competing interest

The authors declare that they have no known competing financial interests or personal relationships that could have appeared to influence the work reported in this paper.

Acknowledgments

This work was financially supported by the National Natural Science Foundation of China (Nos. 42075113, 91961123, 21773249, 42120104007, 21876177), the International Partnership Program of Chinese Academy of Sciences (No. 116134KYSB20170048) and the Key Program of Research and Development of Hefei Science Center, CAS (No. 2020HSCKPRD001). B.L. is grateful to the Science and Technology Foundation of Guizhou Province (No. [2019]5648) and the Science and Technology Foundation of Guizhou Provincial Department of Education (No. KY[2021]014). C.F. would like to thank the CAS President's International Fellowship Initiative (No. 2018VMA0055).

References

Aschmann, S.M., Long, W.D., Atkinson, R., 2006. Temperature-dependent rate constants for the gas-phase reactions of OH radicals with 1,3,5-trimethylbenzene, triethyl phosphate, and a series of alkylphosphonates. J. Phys. Chem. 110, 7393–7400. https://doi.org/10.1021/jp061542r.

Assaf, E., Schoemaecker, C., Vereecken, L., Fittschen, C., 2018. Experimental and theoretical investigation of the reaction of RO_2 radicals with OH radicals: dependence of the HO_2 yield on the size of the alkyl group. Int. J. Chem. Kinet. 50, 670–680. https://doi.org/10.1002/kin.21191.

Assaf, E., Song, B., Tomas, A., Schoemaecker, C., Fittschen, C., 2016. Rate constant of the reaction between CH_3O_2 radicals and OH radicals revisited. J. Phys. Chem. 120, 8923–8932. https://doi.org/10.1021/acs.jpca.6b07704.

Bloss, C., Wagner, V., Jenkin, M.E., Volkamer, R., Bloss, W.J., Lee, J.D., Heard, D.E., Wirtz, K., Martin-Reviejo, M., Rea, G., Wenger, J.C., Pilling, M.J., 2005. Development of a detailed chemical mechanism (MCMv3.1) for the atmospheric oxidation of aromatic hydrocarbons. Atmos. Chem. Phys. 5, 641–664. https://doi.org/10.5194/acp-5-641-2005.

Caravan, R.L., Khan, M.A.H., Zádor, J., Sheps, L., Antonov, I.O., Rotavera, B., Ramasesha, K., Au, K., Chen, M.-W., Rösch, D., Osborn, D.L., Fittschen, C., Schoemaecker, C., Duncianu, M., Grira, A., Dusanter, S., Tomas, A., Percival, C.J., Shallcross, D.E., Taatjes, C.A., 2018. The reaction of hydroxyl and methylperoxy radicals is not a major source of atmospheric methanol. Nat. Commun. 9, 4343. https://doi.org/10.1038/s41467-018-06716-x.

Dommen, J., Prevot, A.S.H., Baertsch-Ritter, N., Maffeis, G., Longoni, M.G., Grüebler, F.C., Thielmann, A., 2003. High-resolution emission inventory of the Lombardy region: development and comparison with measurements. Atmos. Environ. 37, 4149–4161. https://doi.org/10.1016/S1352-2310(03)00507-7.

Duncan, W.T., Bell, R.L., Truong, T.N., 1998. TheRate: program for ab initio direct dynamics calculations of thermal and vibrational-state-selected rate constants. J. Comput. Chem. 19, 1039–1052. https://doi.org/10.1002/(SICI)1096-987X(19980715)19:9<1039::AID-JCC5>3.0.CO;2-R.

Eyring, H., 1935. The activated complex in chemical reactions. J. Chem. Phys. 3, 107–115. https://doi.org/10.1063/1.1749604.

Faragó, E.P., Schoemaecker, C., Viskolcz, B., Fittschen, C., 2015. Experimental determination of the rate constant of the reaction between $C_2H_5O_2$ and OH radicals. Chem. Phys. Lett. 619, 196–200. https://doi.org/10.1016/j.cplett.2014.11.069.

Fernández-Ramos, A., Miller, J.A., Klippenstein, S.J., Truhlar, D.G., 2006. Modeling the kinetics of bimolecular reactions. Chem. Rev. 106, 4518–4584. https://doi.org/10.1021/cr050205w.

Frisch, M.J., Trucks, G.W., Schlegel, H.B., Scuseria, G.E., Robb, M.A., Cheeseman, J.R., Scalmani, G., Barone, V., Petersson, G.A., Nakatsuji, H., et al., 2016. Gaussian 16, Revision A.03. Gaussian, Inc., Wallingford CT.

Gai, Y., Lin, X., Ma, Q., Hu, C., Gu, X., Zhao, W., Fang, B., Zhang, W., Long, B., Long, Z., 2015. Experimental and theoretical study of reactions of OH radicals with hexenols: an evaluation of the relative importance of the H-abstraction reaction channel. Environ. Sci. Technol. 49, 10380–10388. https://doi.org/10.1021/acs.est.5b01682.

Gonzalez, C., Schlegel, H.B., 1989. An improved algorithm for reaction path following. J. Chem. Phys. 90, 2154–2161. https://doi.org/10.1063/1.456010.

Gonzalez, C., Schlegel, H.B., 1990. Reaction path following in mass-weighted internal coordinates. J. Phys. Chem. 94, 5523–5527. https://doi.org/10.1021/j100377a021.

Hallquist, M., Wenger, J.C., Baltensperger, U., Rudich, Y., Simpson, D., Claeys, M., Dommen, J., Donahue, N.M., George, C., Goldstein, A.H., Hamilton, J.F., Herrmann, H., Hoffmann, T., Iinuma, Y., Jang, M., Jenkin, M.E., Jimenez, J.L., Kiendler-Scharr, A., Maenhaut, W., McFiggans, G., Mentel, T.F., Monod, A., Prévôt, A.S.H., Seinfeld, J.H., Surratt, J.D., Szmigielski, R., Wildt, J., 2009. The formation, properties and impact of secondary organic aerosol: current and emerging issues. Atmos. Chem. Phys. 9, 5155–5236. https://doi.org/10.5194/acp-9-5155-2009.

Jenkin, M.E., Saunders, S.M., Wagner, V., Pilling, M.J., 2003. Protocol for the development of the Master Chemical Mechanism, MCM v3 (Part B): tropospheric degradation of aromatic volatile organic compounds. Atmos. Chem. Phys. 3, 181–193.

Kroll, J.H., Seinfeld, J.H., 2008. Chemistry of secondary organic aerosol: formation and evolution of low-volatility organics in the atmosphere. Atmos. Environ. 42, 3593–3624. https://doi.org/10.1016/j.atmosenv.2008.01.003.

Lin, X., Yang, Z., Yu, H., Gai, Y., Zhang, W., 2019. Mechanism and kinetics of the atmospheric reaction of 1,3,5-trimethylbenzene bicyclic peroxy radical with OH. RSC Adv. 9, 32594–32600. https://doi.org/10.1039/C9RA06562H.

Lin, X., Tang, X., Wen, Z., Long, B., Fittschen, C., Gu, X., Zhang, Y., Zhang, W., 2021. Data of chemical composition of the particles from OH-initiated oxidation of 1,3,5-trimethylbenzene. Data Brief (xx, xxx-xxx).

Ma, P., Zhang, P., Shu, J., Yang, B., Zhang, H., 2018. Characterization of secondary organic aerosol from photo-oxidation of gasoline exhaust and specific sources of major components. Environ. Pollut. 232, 65–72. https://doi.org/10.1016/j.envpol.2017.09.018.

Mehra, A., Wang, Y., Krechmer, J.E., Lambe, A., Majluf, F., Morris, M.A., Priestley, M., Bannan, T.J., Bryant, D.J., Pereira, K.L., Hamilton, J.F., Rickard, A.R., Newland, M.J., Stark, H., Croteau, P., Jayne, J.T., Worsnop, D.R., Canagaratna, M.R., Wang, L., Coe, H., 2020. Evaluation of the chemical composition of gas- and particle-phase products of aromatic oxidation. Atmos. Chem. Phys. 20, 9783–9803. https://doi.org/10.5194/acp-20-9783-2020.

Molina, L.T., Kolb, C.E., de Foy, B., Lamb, B.K., Brune, W.H., Jimenez, J.L., Ramos-Villegas, R., Sarmiento, J., Paramo-Figueroa, V.H., Cardenas, B., Gutierrez-Avedoy, V., Molina, M.J., 2007. Air quality in North America's most populous city - overview of the MCMA-2003 campaign. Atmos. Chem. Phys. 7, 2447–2473. https://doi.org/

10.5194/acp-7-2447-2007.
Orlando, J.J., Tyndall, G.S., 2012. Laboratory studies of organic peroxy radical chemistry: an overview with emphasis on recent issues of atmospheric significance. Chem. Soc. Rev. 41, 6294–6317. https://doi.org/10.1039/C2CS35166H.
Ponnusamy, S., Sandhiya, L., Senthilkumar, K., 2017. The atmospheric oxidation mechanism and kinetics of 1,3,5-trimethylbenzene initiated by OH radicals – a theoretical study. New J. Chem. 41, 10259–10271. https://doi.org/10.1039/C7NJ01285C.
Steinfeld, J., Francisco, J.S., Hase, W.L., 1999. Chemical Kinetics and Dynamics. Prentice Hall, Upper Saddle River, N.J.
Truhlar, D.G., Garrett, B.C., Klippenstein, S.J., 1996. Current status of transition-state theory. J. Phys. Chem. 100, 12771–12800. https://doi.org/10.1021/jp953748q.
Vega, E., Sánchez-Reyna, G., Mora-Perdomo, V., Iglesias, G.S., Arriaga, J.L., Limón-Sánchez, T., Escalona-Segura, S., Gonzalez-Avalos, E., 2011. Air quality assessment in a highly industrialized area of Mexico: concentrations and sources of volatile organic compounds. Fuel 90, 3509–3520. https://doi.org/10.1016/j.fuel.2011.03.050.
Velasco, E., Lamb, B., Westberg, H., Allwine, E., Sosa, G., Arriaga-Colina, J.L., Jobson, B.T., Alexander, M.L., Prazeller, P., Knighton, W.B., Rogers, T.M., Grutter, M., Herndon, S.C., Kolb, C.E., Zavala, M., de Foy, B., Volkamer, R., Molina, L.T., Molina, M.J., 2007. Distribution, magnitudes, reactivities, ratios and diurnal patterns of volatile organic compounds in the Valley of Mexico during the MCMA 2002 & 2003 field campaigns. Atmos. Chem. Phys. 7, 329–353. https://doi.org/10.5194/acp-7-329-2007.
Wang, Y., Mehra, A., Krechmer, J.E., Yang, G., Hu, X., Lu, Y., Lambe, A., Canagaratna, M., Chen, J., Worsnop, D., Coe, H., Wang, L., 2020. Oxygenated products formed from OH-initiated reactions of trimethylbenzene: autoxidation and accretion. Atmos. Chem. Phys. 20, 9563–9579. https://doi.org/10.5194/acp-20-9563-2020.
Wen, Z.-Y., Tang, X.-F., Wang, T., Gu, X.-J., Zhang, W.-J., 2020a. Detection of chemical compositions of ultrafine nanoparticles by a vacuum ultraviolet photoionization nucleation aerosol mass spectrometer. Chin. J. Anal. Chem. 48, 491–497. https://doi.org/10.1016/S1872-2040(20)60009-3.
Wen, Z., Tang, X., Fittschen, C., Zhang, C., Wang, T., Wang, C., Gu, X., Zhang, W., 2020b. Online analysis of gas-phase radical reactions using vacuum ultraviolet lamp photoionization and time-of-flight mass spectrometry. Rev. Sci. Instrum. 91, 043201. https://doi.org/10.1063/1.5135387.
Werner, H.J., Knowles, P.J., 2012. MOLPRO, Version 2012.1, a Package of Ab Initio Program.
Wyche, K.P., Monks, P.S., Ellis, A.M., Cordell, R.L., Parker, A.E., Whyte, C., Metzger, A., Dommen, J., Duplissy, J., Prevot, A.S.H., Baltensperger, U., Rickard, A.R., Wulfert, F., 2009. Gas phase precursors to anthropogenic secondary organic aerosol: detailed observations of 1,3,5-trimethylbenzene photooxidation. Atmos. Chem. Phys. 9, 635–665. https://doi.org/10.5194/acp-9-635-2009.
Yan, C., Kocevska, S., Krasnoperov, L.N., 2016. Kinetics of the reaction of CH_3O_2 radicals with OH studied over the 292–526 K temperature range. J. Phys. Chem. 120, 6111–6121. https://doi.org/10.1021/acs.jpca.6b04213.
Zhang, S., Truong, T.N., 2001. VKLab, Version 1.0. University of Utah, Salt Lake City, UT.